Hindawi Publishing Corporation
International Journal of Distributed Sensor Networks
Volume 2015, Article ID 256162, 11 pages
http://dx.doi.org/10.1155/2015/256162

Research Article

Enhancing the Performance of Indoor Device-Free Passive Localization

Wu Yang,[1] Liangyi Gong,[1] Dapeng Man,[1] Jiguang Lv,[1] Haibin Cai,[2] Xiancun Zhou,[3] and Zheng Yang[4]

[1]*Department of Computer Science & Technology, Harbin Engineering University, Harbin 150001, China*
[2]*Software Engineering Institute, East China Normal University, Shanghai 200062, China*
[3]*Department of Information Engineering, West Anhui University, Lu'an 237012, China*
[4]*School of Software and TNList, Tsinghua University, Beijing 100084, China*

Correspondence should be addressed to Liangyi Gong; gongliangyi@hrbeu.edu.cn

Received 19 January 2015; Accepted 1 July 2015

Academic Editor: Chen Qian

Device-free passive localization (DFPL) has been an emerging application with fast increasing development. Channel State Information- (CSI-) based DFPL is recently paid more attention to for fine-granularity and stability of CSI. However, lots of dead spots exist in the area of interest. And the accuracy of localization is not still completely satisfactory, especially for outside of the first Fresnel zone. In our paper, we put forward a new metric to estimate the sensitivity of a receiver to changes in the detecting area. In our experiment, we observe that the performance of DFPL can be raised when the receiver is placed at the location with high receiver sensitivity. Hence, we develop a new high-performance indoor device-free passive localization (HiDFPL), which employs a Bayesian a posteriori approach and possesses high receiver sensitivity. The experiment results demonstrate the outstanding performance of the proposed scheme.

1. Introduction

Location-aware service offers great convenience to people's life. Notably, device-free passive localization (DFPL) without the need for carrying any electronic device plays an important role in many application areas, such as security and surveillance and assisted living and elder care. Recently, a larger number of advanced DFPL applications are researched and developed [1–5]. In this paper, based on lots of experimental observation, we put forward a novel fine-grained device-free passive localization with high sensitivity and accuracy.

DFPL originally employed easy-access radio signal strength indicator (RSSI) as signal features [6]. Most of DFPL systems achieve human locations using data fusion technology based on the effect of human shadowing. However, in the indoor environment with serious multipaths effect, RSSI is variable and insensitive for moving human that is far from the line link [5]. Hence, the accuracy of DFPL relies on lots of limited conditions, such as intensive equipment deployment and site-survey fingerprinting. Aiming to realize high-accuracy DFPL, some researchers explored utilizing of wireless physical layer information. Channel State Information (CSI) is a common and fine-grained signal feature, which can characterise the multipath propagation and be helpful to high-accuracy DFPL.

Recently, with the WLAN and OFDM technology development, DFPL based on CSI is paid more attention to [7]. MonoPHY [3] and Pilot [4] systems firstly achieve CSI-based DFPL with a few pieces of equipment (even only a transmitter-receiver pair). However, it is observed that numerous dead spots exist in the area of interest. At the same time, the accuracy of DFPL is not yet completely satisfactory, especially for outsides of first Fresnel zone. The common solution to reduce dead spots and guarantee good performance is to increase transmitter-receiver pairs so that the area of interest is filled with more wireless signal. However, that will cause more cost including time, power, and money. Now, how to use the least transmitter-receiver pairs to achieve a high-accuracy device-free passive localization with as less as possible dead spots is a problem.

Therefore, we constructed a large number of experiments with a transmitter-receiver pair. To our surprise, it is observed that the receiver possesses diverse sensitivity to environment changes when the receiver is placed at different locations. Through our analysis and discussion, we agree that the received signals from different locations contain different richness of multipath radio signal arriving at the receiver with clusters. Moreover, when the receiver locates different locations, the phase shift of signal due to reflection and scattering causes constructive and destructive multipath interference. Hence, when the receiver is placed at the location with high receiver sensitivity, it is feasible to achieve a high-accuracy DFPL with the least dead spots.

In the communication community, Rician K factor is defined as the power ration between the LOS and NLOS paths to indict the richness of multipath propagation [8]. But an estimator for Rician K factor relies on accurate phase, which is difficultly extracted on commercial WiFi devices [9, 10]. Hence, how to estimate the richness of multipath propagation on commercial wireless cards is a challenge. We noticed that CSI possesses finer-grained frequency resolution and higher time resolution to distinguish multipath components. So, we explored leveraging of CSI from commercial wireless cards to estimate the richness of multipath components [11]. Through plenty of experiments, we observed that when the receiver sensitivity is high, the kurtosis of standard deviation of all subcarriers' amplitudes is small but its mean is large. Combined with the theory and experiments, we propose a novel K_s factor to estimate receiver sensitivity.

In this paper, a high-performance indoor device-free passive localization (HiDFPL) is proposed. The HiDFPL takes advantage of CSI to evaluate a receiver sensitivity and search for a high-sensitive receiver location for reducing the number of dead spots. Experimental evaluation in typical indoor scenarios shows that HiDFPL can achieve an accuracy of 0.79 m. This corresponds to at least 20% enhancement in distance error over the state-of-the-art DFPL systems.

The main contributions of HiDFPL system are summarized as follows.

(1) We propose a high-performance indoor device-free passive localization system. It can cover a larger area of interest and observably improve the accuracy of localization.

(2) To the best of our knowledge, this is a novel work to estimate the sensitivity of indoor receivers based on commercial wireless cards, which is helpful to improve the performance of DFPL system.

(3) Extensive evaluation of HiDFPL with commercial 802.11n NICs is constructed in two typical indoor scenarios. These measurements show that the HiDFPL can greatly reduce the number of dead spots in the area of interest and achieve at least 20% enhancement in median error over the state-of-the-art DFPL systems using the same WLAN installation.

In the rest of the paper, we first provide a preliminary in Section 2 and detail the receiver sensitivity in Section 3. Then our scheme is descripted in Section 4. Section 5 presents the performance evaluation; Section 6 discusses the related work. Finally, Section 7 concludes our work.

2. Preliminary

2.1. Channel State Information. Orthogonal frequency division multiplexing (OFDM) [12] is a promising technology mitigating the effects of frequency selectivity and ISL. In 802.11n standard that employs the OFDM technology, channel is divided into multiple subcarriers. It can be modeled as follows:

$$Y = H * X + n, \tag{1}$$

where X is a transmitted symbol, Y is a received symbol, n is noise, H is Channel State Information (CSI) that is reported as a complex channel transfer matrix representing the channel gain for all subcarriers [13].

CSI refers to known channel properties of a communication link from the transmitter(s) to the receiver(s). CSI is shown as a set of measurements depicting the amplitude and phase of every subcarrier in the channel of OFDM system. CSI is mathematically represented as $h = |h|e^{j(\angle h)}$, which can be extended to matrix values depending on the number of antenna elements. Some commercial wireless cards, such as Intel 5300 NICs, can export a group of discrete channel frequency responses (CFRs) on 30 subcarriers to driver in the format of CSI.

2.2. Indoor Radio Propagation Model. Different from outdoor space, signals of the indoor contain the larger number of multipath signals. In typical indoor scenarios, a transmitted signal propagates to the receiver through reflection, scattering, and attenuation. Each multipath signal introduces different time delay, amplitude attenuation, and phase shift [14]. Hence, the channel impulse response of received signal can be expressed as

$$h(t) = \sum_{i=1}^{N} \alpha_i(t)\, e^{-j\phi_i(t)} \delta\left(\tau - \tau_i(t)\right), \tag{2}$$

where N is number of multipath signals and $\alpha_i(t)$, $\phi_i(t) = 2\pi f \tau_t(t)$, and $\tau_i(t)$, respectively, represent the amplitude, phase, and time delay of the ith multipath component. The channel impulse response in (2) can be obtained by applying a fast Fourier transform, the CFR. If there is a Line-of-Sight (LOS) path, (2) is given by

$$h(t) = \alpha_{\mathrm{LOS}} e^{-j\phi_{\mathrm{LOS}}} + \sum_{i=1}^{N-1} \alpha_{r,i}(t)\, e^{-j\phi_{r,i}(t)}, \tag{3}$$

where $\alpha_r(t)$, $\phi_r(t)$ are the amplitude and phase of multipath signals.

The value of α is related to reflection coefficients. Electromagnetic material causes more serious signal attenuation, while, for the same material, signals of different frequencies suffer from different power loss. The signal of high frequency is too severely attenuated to be detected by the receiver. The phase shift $\Delta\phi_r = |\phi_r - \phi_0| = 2\pi f \Delta d/c$ is related to locations of an obstacle. When the obstacle is close to the LOS path, the phase shift is smaller.

3. Receiver Sensitivity

In multipath-rich indoor environments, wireless signals can transmit to the receiver via reflection, diffraction, and scattering [15]. Human appearance or motions tend to alter signal propagation in a more sophisticated manner, leading to different sensing levels at the receiver. In this paper, a receiver sensitivity is put forward as an evaluation for an ability of receiver to sense changes of signal propagation in an indoor region. Generally, the sensing region is characterized by an ellipse along the transmitter-receiver (TX-RX) link [16], known as Fresnel zone. The receiver has the highest sensitivity to changes in the first Fresnel zone. With the zone being larger, the receiver sensitivity is more and more feebler.

Compared with the RSSI, the CSI is fine-grained and owns high sensitivity to changes of the surrounding. Pilot and MonoPHY systems have significant performance in device-free passive localization. However, some works still need to be solved for device-free passive localization.

(1) Some dead spots exist in an area of interest.

(2) For the indoor environment, the accuracy of localization can be further improved.

As previously discussed, receivers at different locations can exhibit different sensitivity levels to the same human appearance or motions. For different receiver locations, multipath components can superpose either constructively or destructively [17], and the ratio of the Non-Line-of-Sight (NLOS) paths in the total received signals also varies. With larger number of multipath signals, human body is potential to disturb many reflected rays paths, resulting in more severe fluctuations of the received signals. In contrast, with a strong LOS ray, human can only disturb significantly the receiver signal in close proximity to the direct path. Hence, human on a NLOS location tends to induce inapparent changes of the received signals. Therefore, the receiver sensitivity level is closely related to the proportion of the NLOS rays in the received signals.

Theoretically, the received envelope r follows Rician distribution; then it can be depicted by Rician K factor as follows [18]:

$$p(r) = \frac{2(K+1)r}{\Omega} e^{(-K-(K+1)r^2/\Omega)} I_0\left(2r\sqrt{\frac{K(K+1)}{\Omega}}\right), \quad (4)$$

where $I_0(\cdot)$ is the zero-order modified Bessel function of the first kind and Ω denotes the total received power. Though the Rician K can be calculated by the phase information on special electronic instruments, it is difficult for common commercial WiFi equipment, due to lack of time and phase synchronization [19]. Fortunately, we observed that the statistical features of CSI amplitudes can be employed to indict the richness of multipath propagation [15]. The reasons are twofold.

(1) The attenuation of reflection and scattering signals relates to the frequency. Generally, the signal of high frequency suffers more serious fading than that of low frequency.

(2) When NLOS signals are rich, amplitudes of receiver signals can be obviously effected by the reflection and scattering along the paths.

In ideal conditions, amplitudes on subcarriers of OFDM signals are almost the same. Therefore, we can presume that, in case of only a stronger LOS path, amplitudes on subcarriers remain similar if normalized to the same frequency after propagating through the same path. In contrast, in case of rich NLOS signals, signals of high frequencies are too severely attenuated. The amplitudes of signals subcarriers deviate from each other even when normalized to the same frequency [19]. Hence, we collect CSI and normalize the CSI amplitude of each subcarrier to the central carrier frequency f_c as follows:

$$H_{\text{norm}}(f_k) = \frac{f_k}{f_c} \cdot H(f_k), \quad (5)$$

where $H(f_k)$ and $H_{\text{norm}}(f_k)$ are the original and normalized (with respect to f_c) amplitudes of the kth subcarrier. f_k is the frequency of the kth subcarrier. To further eliminate the impact of measurement scales and obtain a dimensionless quantity, we calculate the coefficient of variation of the normalized CSI amplitudes as follows:

$$\text{cv} = \frac{\text{std}(H_{\text{norm}})}{\text{mean}(H_{\text{norm}})}, \quad (6)$$

where $\text{std}(H_{\text{norm}})$ and $\text{mean}_{\text{norm}}$ are the standard deviation and mean of the normalized CSI amplitudes H_{norm}, respectively. Figure 1 shows the distributions of the coefficient of variation. As is shown, the cv values under low sensitivity are smaller and possess a narrower distribution. To quantify the difference of cv distributions, we employ a new metric K_s as follows:

$$K_s = \frac{\kappa}{\mu}, \quad (7)$$

where κ and μ denote the kurtosis and mean of the cv values, respectively.

To validate the effectiveness of (7), we conduct the following measurements. As shown in Figure 2, we fix the location of the transmitter and place the receiver at different locations. For each receiver location, we let a person walk within A and B and collect 6000 data packets. We also collect the same amount of packets when there is no person in the monitored area. In order to qualitatively estimate receiver sensitivity, we employ the detection approach of *Pilot* system. Then we rank the sensitivity of these receiver locations into three levels and mark the sensitivity levels. As is shown in Figure 2, at different receiver locations, since the richness of multipath propagation differs, the sensitivity level to human motions also varies. We then calculate the K_s values for each receiver location using data collected when there is no person in the monitored area. We also calculate the Rician K factors using the same measurements. Table 1 lists the K_s values, Rician K

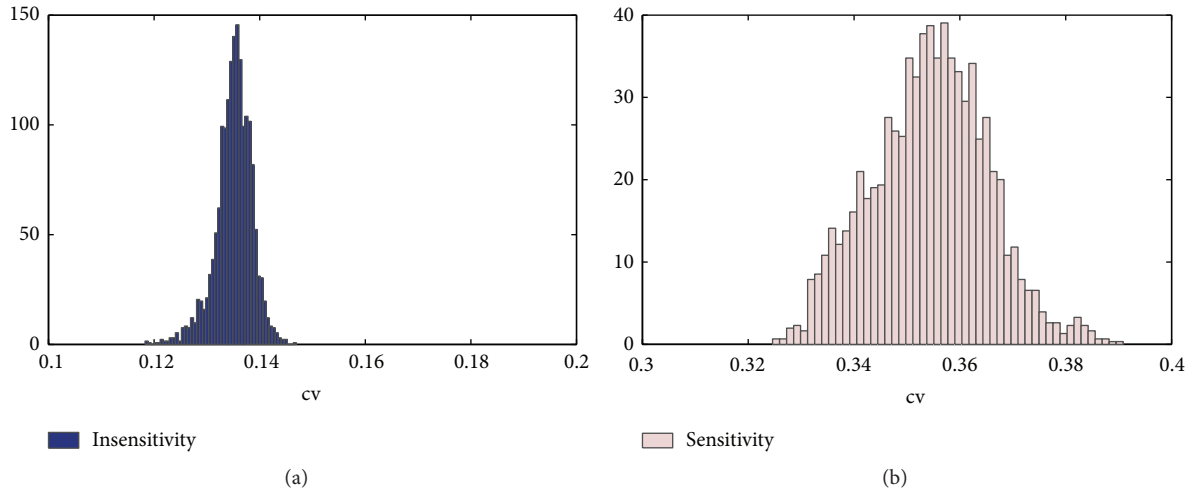

Figure 1: Distributions of the cv values under different sensitivity.

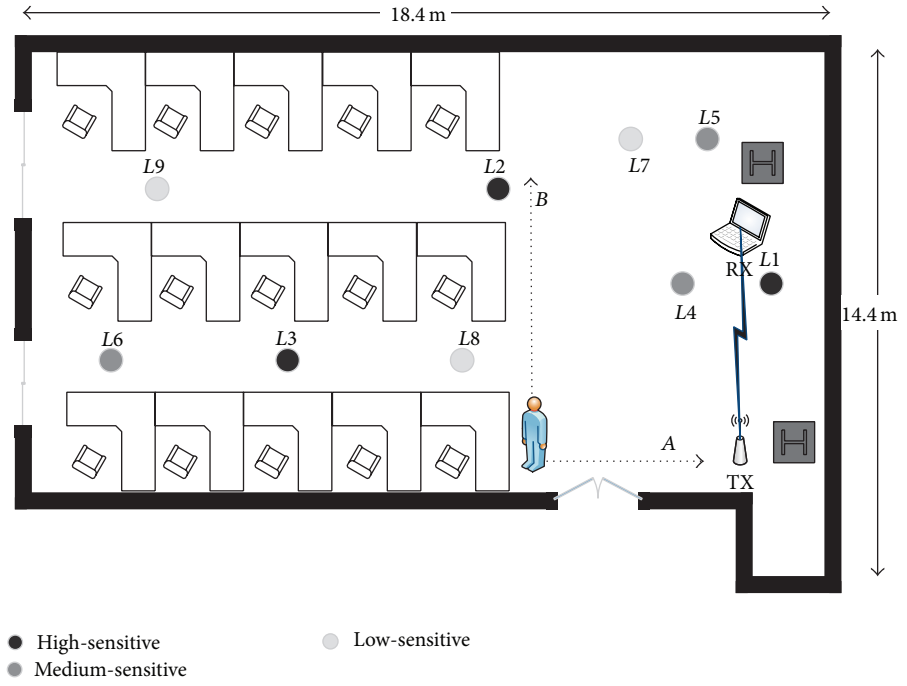

Figure 2: Measurement setup of K_s.

factors [18], and the corresponding sensitivity levels for each tested receiver location. As is shown, the K_s values roughly increase monotonously with the decrease of sensitivity levels at each receiver location. In contrast, no notable trend can be seen between the Rician K factors and the sensitivity levels. We thus employ the K_s value as an indicator for the multipath propagation conditions, which further quantify the sensitivity level of the receiver location.

4. The System Design

In the section, we expound the design of our system. Firstly, we present an overview of system architecture. Then we lay out detailed description of each component in the system.

4.1. Overview. HiDFPL is built on the WLAN infrastructures. In our design, HiDFPL system contains three hardware elements: transmitters, receivers, and server. Access points or wireless routers are generally used as the transmitters. Computers with commercial wireless cards are used as the receivers. The receivers send ICMP messages and collect the CSI periodically. The CSI is sent to the server. The server performs detection and localization by carrying out two main phases as shown in Figure 3.

4.1.1. Offline Phase. In the offline phase, passive radio fingerprints database is constructed. Different human locations can cause diverse effects on the propagating signals. Hence, in the phase, workers collect the fingerprints of all locations.

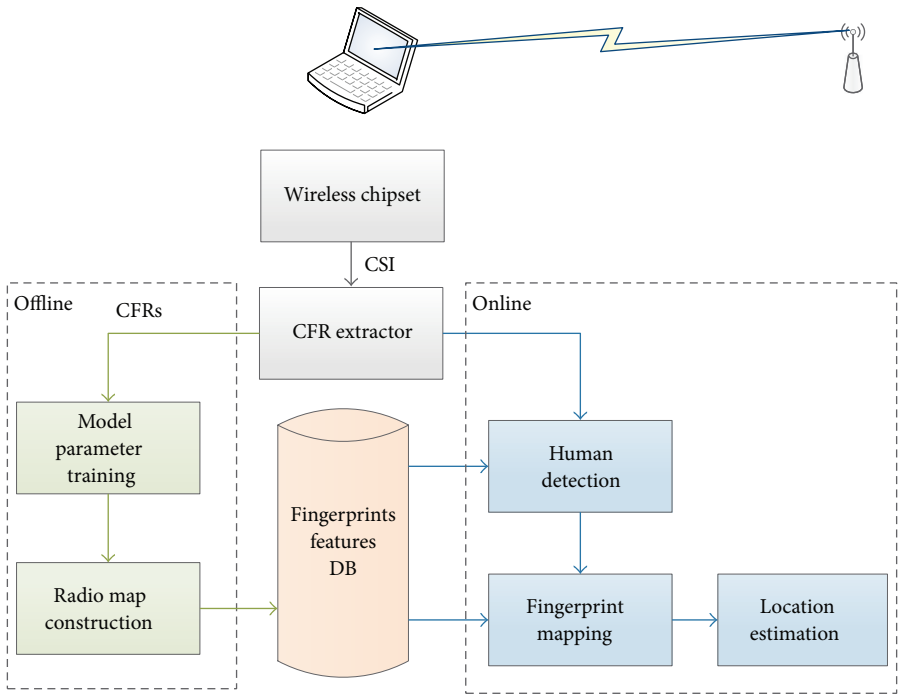

Figure 3: The system architecture.

Table 1: K_s value and Rician K factor versus sensitivity.

RX location	K_s	K factor	Sensitivity
L1	3.89	641.44	High
L2	3.96	31.80	High
L3	4.37	317.36	High
L4	5.01	250.16	Medium
L5	7.27	222.33	Medium
L6	9.26	283.15	Medium
L7	27.41	421.21	Low
L8	13.15	506.84	Low
L9	18.29	285.70	Low

When a person stands at one location, the receivers collect CSI from all transmitters. Then they send the CSI to the server, where CSI is processed and model parameters are calculated. The server stores all model parameters related to the location into the database. In order to detect the appearance of a person, the fingerprints of normal status (nobody) also need to be collected.

4.1.2. Online Phase. In the online phase, the server can detect the appearance of a person and locate his locations in real-time. The receivers send ICMP messages to the transmitters and collect the CSI from response packages. Then the CSI is sent to the server, where CSI is processed. Finally, the server estimates the status and locations of a person through Bayesian maximum a posteriori (MAP) approach.

4.2. System Model. HiDFPL employs a posteriori approach that is well-known probabilistic algorithm for performing fingerprint-based [20] position estimation. It is assumed that the area of interest is a two-dimensional space with the size X. In the area, N locations are collected as fingerprinting points, while, in order to detect the appearance of a person, it needs to collect the signal features when no one exists. Hence, $N+1$ fingerprints are needed to be collected. a groups of transmitter-receiver pairs are deployed in the area. Every transmitter possesses m antennas while each receiver has n antennas. So this leads to a total of $a * m * n$ virtual signal strength links. The receivers can extract the amplitude on each subcarrier from a virtual link as the signal feature.

In the offline phase, a worker stands at the location $x \in X$. The receivers collect all CSI from virtual links. It assumes that l packages are collected. The probability distribution function (PDF) of amplitude on each subcarrier approximately fits a Gaussian distribution mixture nicely [3, 21], as shown in Figure 4. Hence, the PDF of ith virtual link can be considered as

$$f(x) = \frac{1}{2\sigma^2} e^{(x-\mu)^2/\sigma^2}, \tag{8}$$

where μ and σ represent the mean and variance of amplitude. For the ith subcarrier, its fingerprint can be represented by a vector $r^i = (\mu, \sigma)$. It assumes that the number of subcarriers is f. Hence, the fingerprint of each location can be represented by a set $R = r^f_{a,n,m}$.

In the online phase, the receivers collect the CSI in real-time. It is assumed that a receiver extracts an amplitude vector $V = (h^1_{1,1}, h^1_{1,2}, \ldots, h^f_{n,m})$, where h is the amplitude

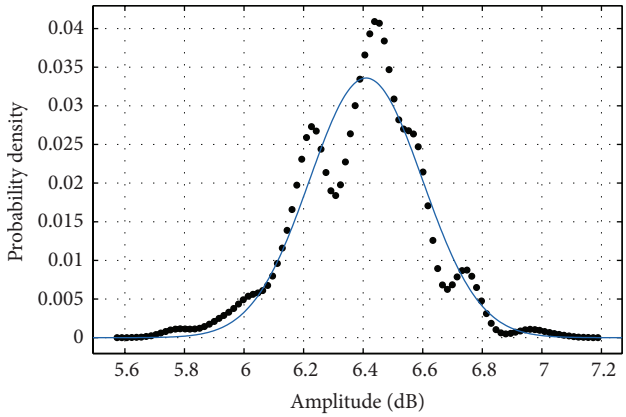

Figure 4: The PDF of amplitude subcarrier.

of the subcarrier. Therefore, the problem becomes, given a vector V, we want to estimate the most probable entity status and location based on the fingerprints database. In the following section, we lay out detailed mathematical models of detection and localization components.

4.3. Detection. Detection component refers to detection of the appearance of an entity in the area of interest. The Probability Density Function (PDF) of amplitude subcarrier approximately fits a Gaussian distribution due to the influence of noise. The noise is random and hard to predict. Hence, we employ a posteriori decision approach to detect appearance of an entity.

In the online phase, a receiver collects CSI and extracts amplitudes of all subcarriers. Given a CSI amplitude vector V, the system matches the fingerprint S of normal status when there is no one. Using a posteriori approach, this can be represented as

$$P(S \mid V) = \frac{P(V \mid S)\, P(S)}{P(V)} > \alpha. \tag{9}$$

Assume normal and abnormal statuses are equally likely and $P(V)$ is independent of status. Hence, (9) becomes

$$P(V \mid S) = \prod_{f} \int f(x) > \beta, \tag{10}$$

where $f(x)$ is the Gaussian density function of normal status and the threshold β can be calculated through training data in the offline phase.

To enhance robustness, we apply (10) on a sequence of packets during a time window w, where the detecting result with the highest vote is returned as the most probable status.

4.3.1. Localization. After an intrusion event occurs, the system starts to locate the intruder. Given a CSI amplitude vector V, the system searches the location L in the fingerprints that maximizes the probability $P(L \mid V)$. That is,

$$L = \arg\max_{L} P(L \mid V). \tag{11}$$

Using Bayesian maximum a posteriori approach, this can be represented as

$$L = \arg\max_{L} \frac{P(V \mid L)\, P(L)}{P(V)}. \tag{12}$$

Assume all locations are equally likely and $P(V)$ is independent of locations. Hence, (12) becomes

$$L = \arg\max_{L} P(V \mid L) \tag{13}$$

and the probability $P(V \mid L)$ can be calculated from the fingerprint database as

$$P(V \mid L) = \arg\max_{L} \prod_{a} \prod_{n} \prod_{m} \prod_{f} \int f(x), \tag{14}$$

where $f(x)$ is the Gaussian density function of a location. For $P(H^{s}_{i,j} \mid l) \in [0, 1]$, $P(H \mid l)$ can be very little with s, i, j increasing. To simplify the calculation and consider that the Napierian logarithm function is a convex function keeping the monotone increasing, we apply the Napierian logarithm function to (14) that goes for (10):

$$\ln P(V \mid L) = \sum_{a} \sum_{n} \sum_{m} \sum_{f} \ln P\left(V^{f} \mid L\right)_{a,n,m}. \tag{15}$$

To increase the robustness of localization estimator, we apply (15) on a sequence of packets during a time widow w. A voting process is employed to estimate the final location of the human with the majority of votes.

In summary, given the CSI measurement, the Gaussian density-based maximum a priori probability algorithm outputs the location L with maximal priori probability. Note that we only locate a single intruder in indoor scenario. Due to intricate indoor multiple effect, the fingerprints of multiple-targets localization are not a linear relationship with those of single-target localization. The localization of multiple persons is more complicated [4]. Hence, the multiple-targets localization is beyond the scope of this paper.

5. Performance Evaluation

In this section, we present detailed evaluations on HiDFPL. We firstly interpret the experiment methodology, followed by detained performance evaluation results in typical indoor environments including multipath-dense scenarios and NLOS propagation.

5.1. Experiment Methodology. We conducted experiments in two typical indoor scenarios. Each testing room is occupied with desks, chairs, and other furniture, creating different extent of multipath propagation. We detail each testing scenario as follows.

Scenario 1. First, we constructed our experiments in a 12.4 m × 7.2 m classroom furnished with rows of desks and chairs. The TX and the RX are placed 10 m away and 1.5 m in height. We chose 59 locations for training and 28 locations for testing according to the floor plan in Figure 5.

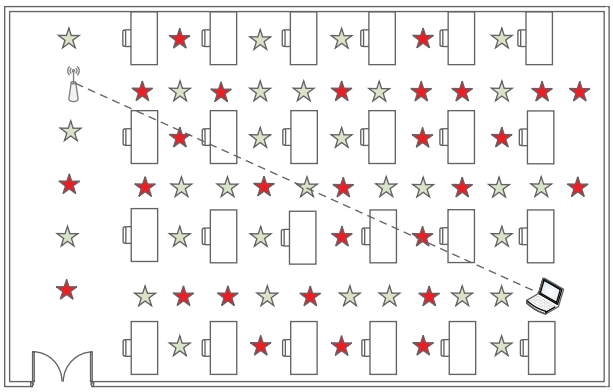

Figure 5: Experiment testbed: classroom.

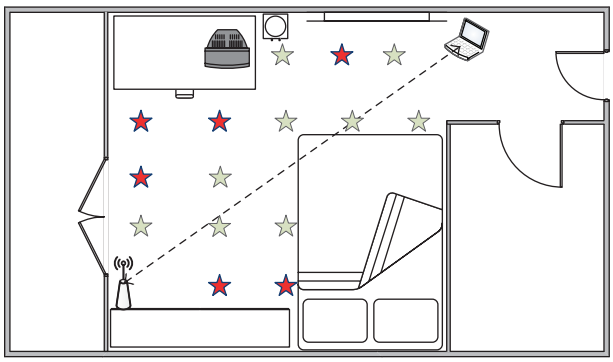

Figure 6: Experiment testbed: home.

Scenario 2. Second, we tested our system in a typical home, which was over approximately 20 m^2. The room was surrounded by various facilities such as desk, chair, bed, bureau, and computer. We placed one pair of TX and RX apart about 4 m, about 0.7 m above the floor. We chose 15 locations for training and 6 locations for testing, as shown in Figure 6.

In our experiments, we considered one pair of TX-RX locations as a link. We employ a single-antenna Tenda W3000R wireless router as the TX operating in IEEE 802.11n AP mode at 2.4 GHz. A LENOVO Thinkpad X200 laptop equipped with Intel 5300 NIC and 2 antennas running Ubuntu 10.04LTS server OS works as the RX pinging packets to the TX. The *iwlwifi* firmware is modified as [8] to start traffic flow and export CSI of each packet. Table 2 shows the default values for different parameters.

During our experiments, we set the transmission rate as 20 packets/second [14]. The experiment using two volunteers was divided into two phases: offline phase and online phase. During the offline phase, the fingerprint database was constructed in one normal case (no one on the link) and a large number of cases of a person standing at training locations (five-pointed star). For each fingerprint training case, we collected CSI for two minutes at different times of day and recorded the CSI amplitudes mean and covariance of 30 subcarriers from different antennas as a location fingerprint. Due to the difference of different human sizes, the Gaussian probability density of every subcarrier amplitude is distorted by different workers. In order to eliminate the diversity of fingerprints of different workers, we employ a linear transferring scheme [22] to transfer the measurement of every subcarrier amplitude across different workers from one location to a feature space, where the distributions of amplitude at one location are as close as possible. During the online phase, we measured CSI a score of times for about 6 seconds [14] at each testing location (red five-pointed star) on the link.

Table 2: Default parameters of HiDFPL system.

Parameter	Default value	Meaning
n	2	Number of RX antennas
m	1	Number of TX antennas
w	2	Time window size
f	30	Number of subcarriers

5.2. Performance Comparison and Analysis. In the section, we firstly evaluate the component performance of the proposed HiDFPL system. Then we analyze the effect of different parameters on the system performance. As shown in Table 2, three types of parameters play an important role in our system. Detailed analysis is represented as follows.

5.2.1. Detection Performance. Anomaly detection aims to detect the appearance of human in area of interest. The receiver with high sensitivity is assumed to be able to detect human accurately in a larger range. In our experiment, we firstly adjusted receiver sensitivity and then collected the data when the volunteers stand at different testing locations that are far from the direct path of TX-RX pair. We employ two conventional metrics to evaluate the anomaly detection performance. (1) False Positive (FP) is the probability of cases when receiver lies about an anomaly event when no one appears within detecting range. (2) False Negative (FN) is the probability of cases when the receiver failed to detect an anomaly event. The experiment results are shown in Figure 7. We can observe that the detection performance of the receiver with high sensitivity improves about 80% enhancement in FP and about 70% enhancement in FN over that of the receiver with low sensitivity. The receiver with high sensitivity is able to accurately distinguish a normal and anomaly event due to an obvious threshold. Hence, the results prove that high receiver sensitivity is much helpful to improve the detection performance.

5.2.2. Localization Performance. When the receiver is placed at the location where it owns high sensitivity, the effect of human appearance on wireless signal is more obvious. The localization accuracy of HiDFPL is theoretically higher than that with low sensitivity. In order to prove the assuming, we constructed lots of experiments using only a single TX-RX pair when the receiver owns high or low sensitivity. Figure 8 shows experiment results expressed by cumulative distribution function (CDF) of the distance error. We can

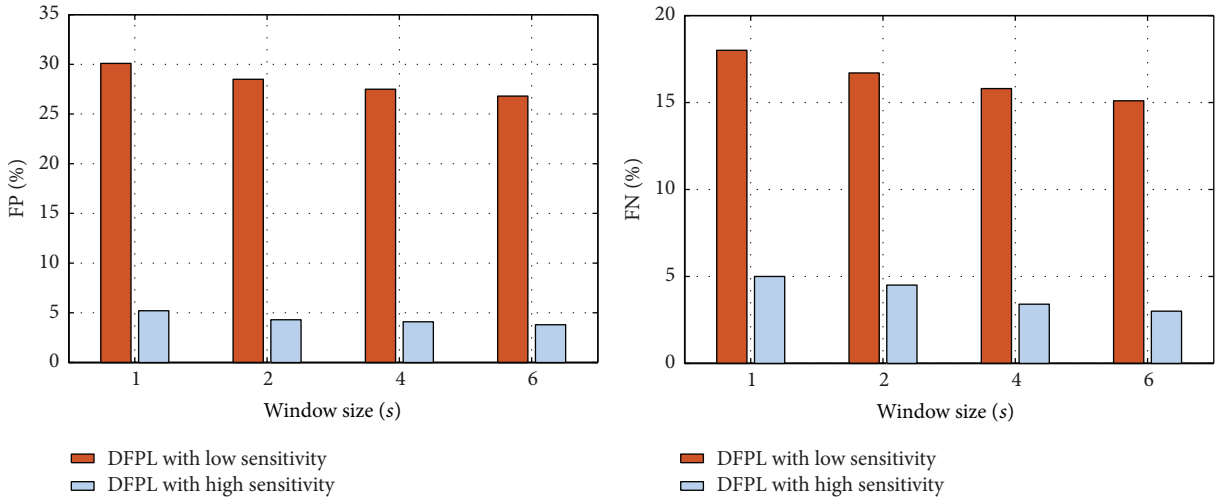

(a) False Positive with different receiver sensitivity

(b) False Negative with different receiver sensitivity

Figure 7: Anomaly detection performance.

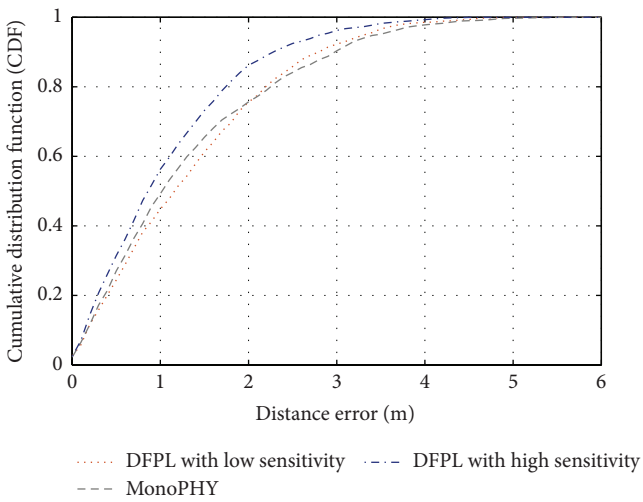

Figure 8: CDF of localization error with different sensitivity.

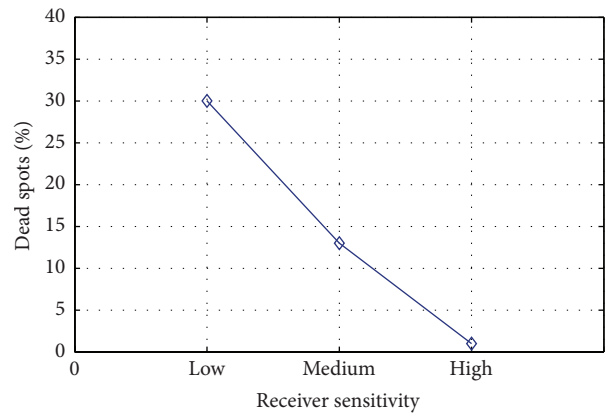

Figure 9: Number of dead spots with different sensitivity.

observe from the figure that the medium distance error of the high-sensitive estimator is 0.79 meters but the medium distance error of the low-sensitive estimator is 1.24 meters. The results also show that HiDFPL has the best accuracy with an enhancement of at least 21% in median distance error over the newest state-of-the-art techniques using only a single TX-RX pair. At the same time, as shown in Figure 9, we can observe that the number of dead spots can reduce with the receiver sensitivity increasing. In a single large room, the dead spots can achieve less than 3% of all training points when the receiver owns high sensitivity. Though some dead spots can be located, the movement of human on those points can be detected. We agree that the HiDFPL has achieved the aim of using a transmitter-receiver pair to achieve a high-accuracy device-free passive localization with as less as possible dead spots.

5.2.3. The Effect of Antennas Number. With the development of WLANs, including IEEE 802.11a/g/n, almost all IEEE 802.11n nodes employ Multiple-Input Multiple-Output (MIMO) technology. MIMO technology not only improves the system throughput and signal transmitting distance, but also possesses plenty of channel information that is used to enhance the performance of localization. In our experiments, we leverage two receiver antennas and evaluate the effect of antennas number on the performance of localization. The evaluation result is shown in Figure 10. In the figure, the result shows that the localization accuracy is discrepant on different antennas and the performance of localization is enhanced by fusing multiple antennas.

5.2.4. The Effect of Time Window Size. Due to the interference of noise, the measurements tinily vary over time, which can cause bad effect on the performance of localization. In the paper, we filter the measurements during a time window to improve the robustness of localization output.

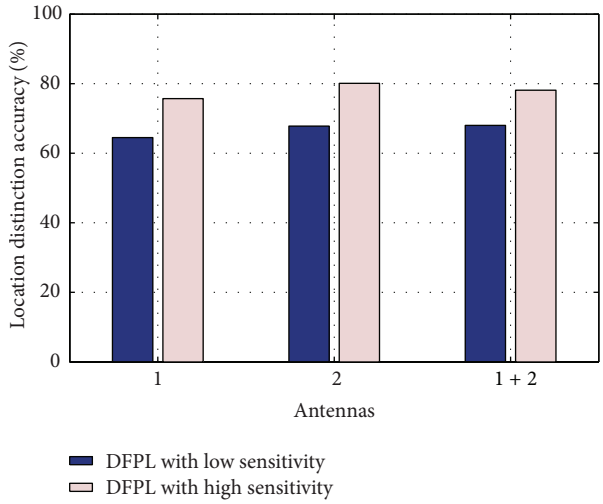

Figure 10: Effect of antenna number.

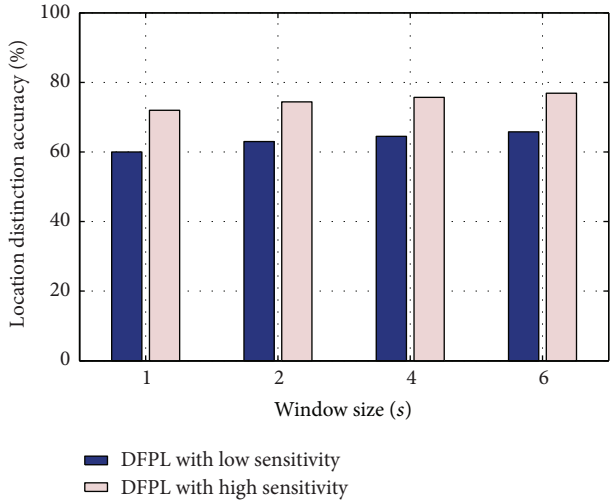

Figure 11: Effect of the time window size.

The experiment results are exhibited in Figure 11. From the figure, we can obviously observe that the performance of localization increases as the time window size enlarges. However, the estimator with a large time window partly reduces the system real-time performance. Therefore, there is a tradeoff between the time window size and the real-time localization.

5.2.5. The Effect of Subcarrier Number. Compared with RSSI, CSI of all subcarriers is a fine-grained feature. The number of subcarriers can cause some effect on the performance of system, including receiver sensitivity estimation and localization accuracy.

As mentioned in Section 3, different subcarriers suffer from varying degrees of fading. It could be helpful to estimate the receiver sensitivity accurately if more subcarriers are employed. We constructed lots of experiments to evaluate the effect of number of subcarriers on the receiver sensitivity.

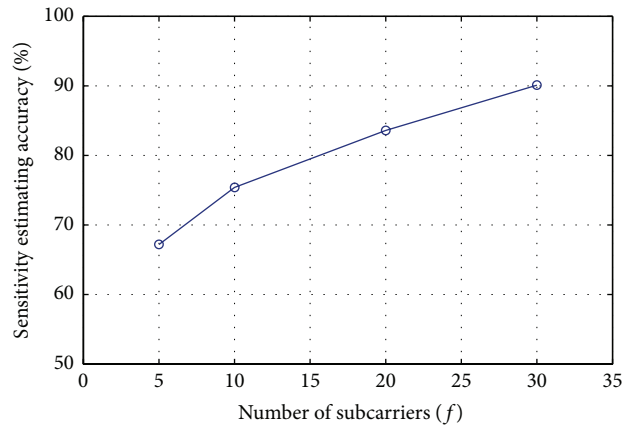

Figure 12: Effect of subcarrier number on sensitivity estimation.

Figure 12 shows that the sensitivity estimation accuracy is raised as the number of subcarrier increases. When we employ 30 subcarriers, the accuracy of receiver sensitivity estimation can achieve about 90%.

Similarly, the number of subcarriers can cause effect on the location distinction accuracy. In our experiments, we, respectively, selected different subcarriers to evaluate the localization accuracy. These subcarriers are evenly spaced as much as possible. The experimental result is shown in Figure 13. From the figure, we can observe that the locations distinction accuracy is improved with the subcarrier number increasing. The performance of system when we used thirty subcarriers is enhanced at least 15% in location distinction accuracy over that when we only used five subcarriers.

6. Related Work

Device-free passive localization (DFPL) refers to detection of the appearance of or further determining of the location of an entity with predeployed monitors, while the entity carries no device. The concept of device-free passive localization was firstly put forward in the literature [23]. In early time, DFPL systems exploited handy feature, such as RSSI, to realize detection, localization, and tracking. Recently, some researchers are exploring the achievement of CSI-based fine-grained DFPL systems.

6.1. RSSI-Based DFPL. Due to the handy access, Received Signal Strength Indicator (RSSI) is early employed in the DFPL. RSSI from MAC layer is coarse-grained and unstable. Hence, most of the RSSI-based DFPL leverage multiple TX-RX pairs to achieve high-accuracy localization. The RSSI-based DFPL takes advantage of two technologies: Radio Tomographic Imaging (RTI) and Fingerprinting Match. Firstly, Wilson and Patwari [24] made use of Radio Tomographic Imaging (RTI) technology to image passive objects based on *Telosb* wireless nodes. Recently, Kaltiokallio et al. [5] found that the spatial impact area varies considerably for each link. Hence, they put forward an online Radio Tomographic Imaging (RTI) system that employs a fade level-based spatial model based on channel diversity to localize and

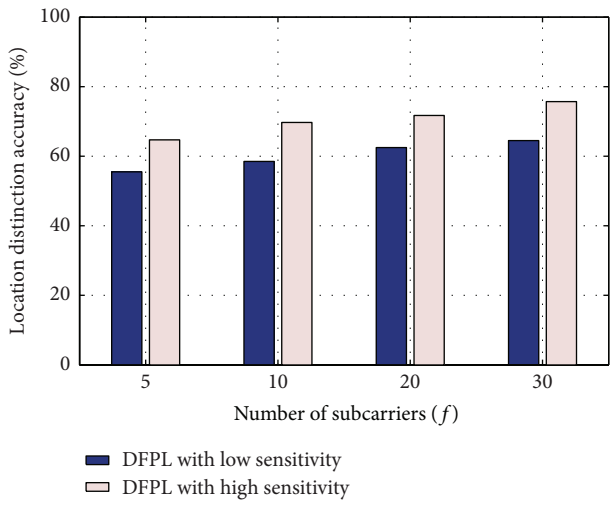

Figure 13: Effect of subcarrier number on localization accuracy.

track a person accurately. Then, in the same manner, Xu et al. [1] employed a fingerprinting-based approach based on RSSI extracted from wireless sensors to locate locations of device-free entities. With the development of WiFi and popularization of WLAN technology, Seifeldin et al. [2] developed a *Nuzzer* system that had high accuracy for large-scale typical environments and required no special hardware and LOS to operate. It works with a low number of streams but needs substantial calibration efforts. Though many researchers pay more attention to the RSSI-based DFPL, the systems are still unsatisfactory due to much cost of deployment and unstable localization performance.

6.2. CSI-Based DFPL. CSI is a fine-grained feature from physical layer, which recently is used to develop indoor DFPL systems. FIMD [25] firstly utilized CSI for device-free passive detection and localization via data fusion with multiple links. Abdel-Nasser et al. [3] developed MonoPHY system as an accurate device-free passive WLAN localization system, which was designed to locate a person in the broad covering area of a monostream. Xiao et al. [4] put forward *Pilot* leveraging temporal stability and frequency otherness of CSI and integrating an anomaly detection block to facilitate the device-free feature. Zhou et al. [14] proposed an omnidirectional passive human detection system through utilizing PHY layer features to virtually tune the shape of monitoring coverage. The system can detect the direction of intruder only relying on a single TX-RX pair. Yang et al. [26] surveyed the difference between CSI and RSSI from various aspects and showed some pioneer works based on CSI that had demonstrated submeter or even centimeter level accuracy. Qian et al. [27] proposed PADS system, a novel device-free passive detection of moving humans with dynamic speed. Both amplitude and phase information of CSI are extracted to be sensitive metrics for target detection. From the experiment results of recent CSI-based DFPL, it can be observed that CSI is helpful to overcome indoor multiple effect and improve the accuracy and stability of DFPL.

7. Conclusion

In this paper, a high-performance indoor device-free passive localization system was proposed, which can achieve a fine-grained localization on a single TX-RX link via fingerprinting. Considering the frequency correlation of signal fading and the otherness of CSI subcarriers, we put forward a receiver sensitive metric based on statistics of CSI features. We propose that the receiver with high sensitivity possessed high accuracy of device-free passive localization. The experiment results show that the HiDFPL can achieve an accuracy of 0.79 m, which corresponds to about 20% enhancement in median distance error over the state-of-the-art MonoPHY and about 36% enhancement in median distance error over the DFPL with low receiver sensitivity. In the next stage, we plan to explore leveraging of CSI phase information to shape more accurate sensitive metric and to employ high receiver sensitivity to realize more fine-grained device-free passive detection and localization.

Conflict of Interests

The authors declare that there is no conflict of interests regarding the publication of this paper.

Acknowledgments

This research is supported by the National Natural Science Foundation of China (Grant nos. 61170242, 61300206, and 61472098) and the Fundamental Research Funds for the Central Universities (Grant no. HEUCF100605).

References

[1] C. Xu, B. Firner, R. S. Moore et al., "Scpl: indoor device-free multi-subject counting and localization using radio signal strength," in *Proceedings of the 12th International Conference on Information Processing in Sensor Networks*, pp. 79–90, ACM, April 2013.

[2] M. Seifeldin, A. Saeed, A. E. Kosba, A. El-Keyi, and M. Youssef, "Nuzzer: a large-scale device-free passive localization system for wireless environments," *IEEE Transactions on Mobile Computing*, vol. 12, no. 7, pp. 1321–1334, 2013.

[3] H. Abdel-Nasser, R. Samir, I. Sabek, and M. Youssef, "MonoPHY: mono-stream-based device-free WLAN localization via physical layer information," in *Proceedings of the IEEE Wireless Communications and Networking Conference (WCNC '13)*, pp. 4546–4551, Shanghai, China, April 2013.

[4] J. Xiao, K. Wu, Y. Yi, L. Wang, and L. M. Ni, "Pilot: passive device-free indoor localization using channel state information," in *Proceedings of the IEEE 33rd International Conference on Distributed Computing Systems (ICDCS '13)*, pp. 236–245, July 2013.

[5] O. Kaltiokallio, M. Bocca, and N. Patwari, "A fade level-based spatial model for radio tomographic imaging," *IEEE Transactions on Mobile Computing*, vol. 13, no. 6, pp. 1159–1172, 2014.

[6] Y. Wen, X. Tian, X. Wang, and S. Lu, "Fundamental limits of rss fingerprinting based indoor localization," in *Proceedings of the*

of IEEE Conference on Computer Communications (INFOCOM '15), Hong Kong, April 2015.

[7] Z. Zhou, C. Wu, Z. Yang, and Y. Liu, "Sensorless sensing with WiFi," *ACM Computing Surveys*, vol. 20, no. 1, pp. 1–6, 2015.

[8] D. Halperin, W. Hu, A. Sheth, and D. Wetherall, "Predictable 802.11 packet delivery from wireless channel measurements," *ACM SIGCOMM Computer Communication Review*, vol. 41, no. 4, pp. 159–170, 2011.

[9] J. Zhang, M. H. Firooz, N. Patwari, and S. K. Kasera, "Advancing wireless link signatures for location distinction," in *Proceedings of the ACM 14th Annual International Conference on Mobile Computing and Networking (MobiCom '08)*, pp. 26–37, September 2008.

[10] S. Sen, B. Radunovic, R. R. Choudhury, and T. Minka, "You are facing the Mona Lisa: spot localization using PHY layer information," in *Proceedings of the 10th International Conference on Mobile Systems, Applications, and Services (MobiSys '12)*, pp. 183–196, ACM, Lake District, UK, June 2012.

[11] Z. Yang, Z. Zhou, and Y. Liu, "From RSSI to CSI: indoor localization via channel response," *ACM Computing Surveys*, vol. 46, no. 2, article 25, 2013.

[12] A. R. Bahai, B. R. Saltzberg, and M. Ergen, *Multi-Carrier Digital Communications: Theory and Applications of OFDM*, Springer, 2004.

[13] S. Sen, J. Lee, K.-H. Kim, and P. Congdon, "Avoiding multipath to revive inbuilding WiFi localization," in *Proceedings of the 11th Annual International Conference on Mobile Systems, Applications, and Services (MobiSys '13)*, pp. 249–262, ACM, June 2013.

[14] Z. Zhou, Z. Yang, C. Wu, L. Shangguan, and Y. Liu, "Omnidirectional coverage for device-free passive human detection," *IEEE Transactions on Parallel and Distributed Systems*, vol. 25, no. 7, pp. 1819–1829, 2014.

[15] T. Rappaport, *Wireless Communications: Principles and Practice*, Prentice Hall, 2nd edition, 2001.

[16] N. Patwari and J. Wilson, "Spatial models for human motion-induced signal strength variance on static links," *IEEE Transactions on Information Forensics and Security*, vol. 6, no. 3, pp. 791–802, 2011.

[17] O. Kaltiokallio, H. Yiğitler, and R. Jäntti, "A three-state received signal strength model for device-free localization," http://arxiv.org/abs/1402.7019.

[18] C. Tepedelenlioğlu, A. Abdi, and G. B. Giannakis, "The Ricean K factor: estimation and performance analysis," *IEEE Transactions on Wireless Communications*, vol. 2, no. 4, pp. 799–810, 2003.

[19] Z. Zhou, Z. Yang, C. Wu, W. Sun, and Y. Liu, "LiFi: Line-Of-Sight identification with WiFi," in *Proceedings of the 33rd IEEE Conference on Computer Communications (INFOCOM '14)*, pp. 2688–2696, May 2014.

[20] J. Han, C. Qian, P. Yang et al., "GenePrint: generic and accurate physical-layer identification for UHF RFID tags," *IEEE/ACM Transactions on Networking*, no. 99, p. 1, 2015.

[21] D. Tse and P. Viswanath, *Fundamentals of Wireless Communication*, Cambridge University Press, Cambridge, UK, 2005.

[22] J. Wang, X. Chen, D. Fang, C. Q. Wu, T. Xing, and W. Nie, "Implications of target diversity for organic device-free localization," in *Proceedings of the 13th International Symposium on Information Processing in Sensor Networks (IPSN '14)*, pp. 279–280, IEEE, April 2014.

[23] M. Youssef, M. Mah, and A. Agrawala, "Challenges: device-free passive localization for wireless environments," in *Proceedings of the 13th Annual ACM International Conference on Mobile Computing and Networking (MobiCom '07)*, pp. 222–229, ACM, September 2007.

[24] J. Wilson and N. Patwari, "Radio tomographic imaging with wireless networks," *IEEE Transactions on Mobile Computing*, vol. 9, no. 5, pp. 621–632, 2010.

[25] J. Xiao, K. Wu, Y. Yi, L. Wang, and L. M. Ni, "FIMD: fine-grained device-free motion detection," in *Proceedings of the 18th IEEE International Conference on Parallel and Distributed Systems (ICPADS '12)*, pp. 229–235, December 2012.

[26] Z. Yang, Z. Zhou, and Y. Liu, "From RSSI to CSI: indoor localization via channel response," *ACM Computing Surveys (CSUR)*, vol. 46, no. 2, article 25, 2013.

[27] K. Qian, C. Wu, Z. Yang, Y. Liu, and Z. Zhou, "PADS: passive detection of moving targets with dynamic speed using PHY layer information," in *Proceedings of the 20th IEEE International Conference on Parallel and Distributed Systems (ICPADS '14)*, pp. 1–8, Hsinchu, Taiwan, December 2014.